The vertical structure of mesoscale eddies in the Azores Current corridor: a combined altimetry-Argo analysis

Susana M. Silva-Fernandes[1] and Álvaro J. Peliz[1]

[1]Instituto Dom Luiz – Faculdade de Ciências, Universidade de Lisboa, Lisboa, Portugal

Correspondence to: Susana Margarida Silva-Fernandes (smsilva@fc.ul.pt)

Abstract. Temperature and salinity, derived from over 10000 Argo profiles, are combined with 20 years of eddy trajectories and absolute dynamic topography maps to characterise the vertical structure of mesoscale eddies within the Azores current corridor (AzCCo) from surface to 1500 dbar. From east to west, our statistics reveal an intensification of the anomaly maxima (from 0.5° C and 0.1 to above 1.5° C and 0.2 of salinity) and a deepening of their core location in the water column (from 250 dbar to 750 dbar) for both anticyclones and cyclones. Anticyclones are characterised by relatively depth-uniform structure, exhibiting warm, salty cores, while cyclones are more vertically structured, with a well-defined subsurface maximum, featuring cold, fresh cores along the AzCCo. These zonal differences are associated with the origins of the sampled eddies and their dynamic properties on either side of the Mid-Atlantic Ridge (MAR). IIn the west, most eddies originate from the Gulf Stream branches, resulting in higher anomaly values. To investigate the mechanisms responsible for these anomalies, an isopycnal decomposition of temperature and salinity anomalies is applied, separating them into two components: heave (HEV), associated with vertical deflections of isopycnal surfaces, and spice (SPI), representing variations along isopycnal surfaces. These components are linked to two main eddy transport mechanisms: eddy pumping and eddy trapping. HEV dominates the resulting vertical structures of temperature and salinity within the water column indicating that most eddy-induced anomalies originate from eddy pumping, manifested as deflections of the isopycnal surfaces. This mechanism produces warmer, saltier anomalies within anticyclonic eddies due to downwelling of the isopycnal surfaces and colder, fresher anomalies within cyclonic eddies due to upwelling of the same surfaces. SPI exhibits higher values within the upper 250 dbar to the east of the MAR, reflecting the tendency of surface eddies to trap different water masses. Finally, absolute values of isopycnal vertical displacement above 50 dbar, from the surface to the 1500 dbar level, demonstrate the significant impact of these mesoscale structures throughout the water column.

1 Introduction

Mesoscale eddies play a crucial role in redistributing heat, salt, and momentum (e.g., Chelton et al., 2011; Treguier et al., 2012; Frenger et al., 2015) by the advection of water masses with distinct thermohaline properties (eddy trapping) from their formation regions to their dissipation sites. In addition, vertical motions induced by mesoscale structures (eddy pumping) influence the transport of nutrients within the water column, while their rotational flow modulates the horizontal distribution of chlorophyll and phytoplankton concentrations (e.g., Martin and Richards, 2001; Gaube et al., 2011; Mahadevan, 2016; Keppler et al., 2024).

The Azores current (AzC) is a highly turbulent zonal jet located around 34° N, east of the Mid-Atlantic ridge (MAR), with mean eddy kinetic energy (EKE) values above 200 $cm^2 s^{-2}$ (Figure 1), the highest of the eastern subtropical North Atlantic. The current system and its associated frontal zone have been revisited several times over the last decades (e.g., Gould, 1985; Juliano and Alves, 2007; Frazão et al., 2022). The latitudinal band surrounding the jet, which we will loosely refer to as the Azores Current Corridor (AzCCo) is characterised by coherent eddies, meanders, and filaments, mostly evolving from baroclinic instability of the jet (Klein and Siedler, 1989; Alves and De Verdière, 1999), as well as several other types of structures propagating into the corridor. Different zonal sectors with distinct characteristics have been identified within the AzCCo, characterised by a decrease in EKE values from west to east. These sectors approximately coincide with the locations of two main topographic features in the region. Furthermore, as the Mid-Atlantic Ridge (MAR) acts as a partial barrier between the basins west and east of the ridge, eddies west of the MAR are not only more energetic but also exhibit larger amplitudes, greater radii, and stronger swirl velocities (see Silva-Fernandes and Peliz, 2020, their Figure 7b), c) and d)). East of the MAR, Barbosa Aguiar et al. (2011) identify three main sectors: (i) the western sector between the MAR and the Seewarte Seamount Chain (SWSM) (~28° W); (ii) the central sector between 28° W and 20° W; and (iii) the eastern sector extending toward the Gulf of Cádiz. While global statistics of the AzC surface eddy field are relatively well known (e.g. Barbosa Aguiar et al., 2011; Silva-Fernandes and Peliz, 2020), a systematic study of the internal structure of these eddies and their impact on the water column is still missing. Existing works comprise mainly isolated events derived from in situ data (e.g., Pingree et al., 1996; Pingree and Sinha, 1998; Mouriño et al., 2002; Mouriño et al., 2003), with most of these studies focusing on the large cyclonic eddies along the "Storm Corridor" (~ 34° N; Pingree, 2002). These large cold-core cyclones are characterised by horizontal temperature anomalies around 2.5° C between 200 and 600 dbar. With a core temperature as low as 3.5° C centred at the 400 dbar level. Also, Pingree et al. (1996) suggested that these eddies have vertical displacements of the isopycnal surfaces of around 200 dbar from the surface to near the bottom (4000 m). Pegliasco et al., 2015 characterised the vertical structure of two clusters of eddies using Argo floats originating in the Canary upwelling system, whose westward propagation partially overlaps the southern flank of the AzCCo (west of 20° W). The surface cluster (cores at ~0–200 m) contains a higher number of anticyclones within the study region, characterised by weak positive anomalies and short propagation trajectories, forming part of the "Canary Corridor" (CnCo). In contrast, the second cluster (eddies with maxima between 200 and 600 m) is dominated by cyclones, which exhibit temperature and salinity anomalies of approximately −0.5 °C and −0.07, respectively, and extend vertically to depths of 600–800 m. This cyclonic cluster reaches longitudes as far as 40° W (near the MAR) and forms part of the "Madeira corridor" (MdCo), previously described by Sangrà et al. (2009). Finally, Amores et al. (2017) used composites of Argo floats and altimetry (Sea Level Anomaly - SLA), covering part of the AzC southern flank (~32°N). They found peak anomalies around 150 m (anticyclones) and at 400-800 m (cyclones), reaching values of potential temperature above 1° C and 0.2 of salinity anomalies for both sign structures, although the cyclones were slightly more intense. Furthermore, the anticyclonic (cyclonic) eddies are generally characterised by warm (cold) and salty (fresher) cores, with their signals reaching a depth of 1200 m.

West of the ridge, based on the trajectories of SOFAR floats launched on both sides of the MAR, (Ollitrault and Colin de Verdière, 2002) , reported that the eddies in that region have a southward flow south of 38º N, usually migrating along the west flank of the ridge. Furthermore, from the tracked eddies, they concluded that cyclones (anticyclones) have cold (warm) cores at 770 dbar.

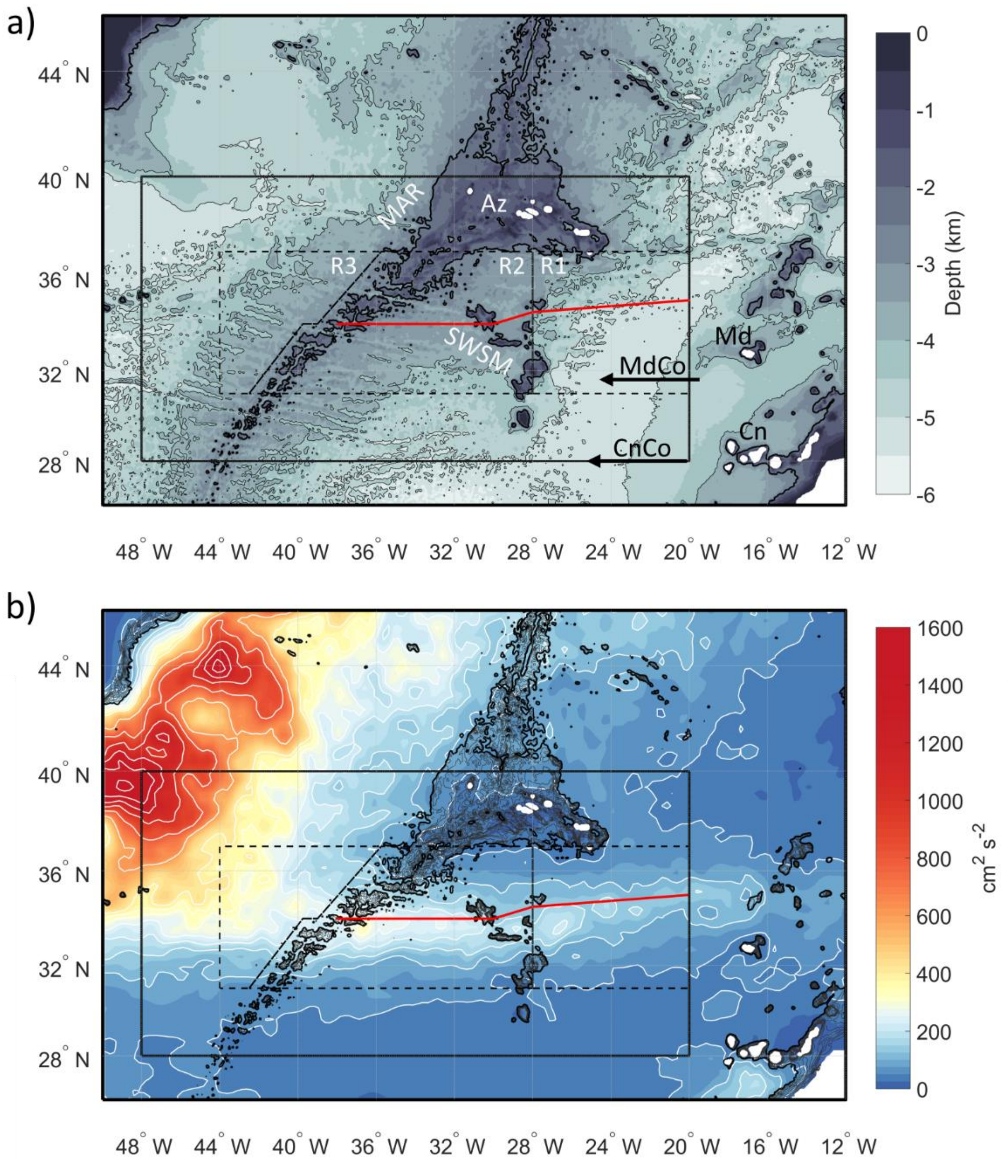

Figure 1: a) Bathymetric map. MAR – Mid-Atlantic Ridge; SWSM – Seewarte Seamount Chain; MdCo – Madeira Corridor; CnCo – Canary Corridor; Md – Madeira Island; Cn – Canary Island; Az – Azores Islands. Bathymetric contours are drawn every 500 m

from the surface down to 6 km depth. The thick black contour represents the 2500 m bathymetric and the black thin ones the 4000 and 5000 m bathymetric. b) Spatial distribution of mean EKE (cm² s⁻²) for the period 2005–2017. Contours are highlighted in white every 50 cm² s⁻² up to 400 cm² s⁻², and then every 200 cm² s⁻² thereafter. Bathymetric contours are drawn every 500 m from the surface down to 2500 m depth. The thick black contour represents the 2500 m bathymetric. In both panels, the black box indicates the study area, and the three dashed boxes represent the regions directly associated with the Azores Current Corridor: the eastern region (R1), the central region (R2), and the western region (R3). The red line represents the mean axis location of the AzC, following Silva-Fernandes and Peliz (2020). Land is shown in white.

Meddies are also encountered east of MAR, especially east of the SWSM and the Azores Plateau (AzP) (Bashmachnikov et al., 2015). As they travel west, their transport of Mediterranean water (MW) with high temperature and salinity (around the 800-1200 dbar levels) results in anomalies that can be easily tracked as they present temperature anomalies above 0.5° C and in salinity above 0.2 for a 200 m layer between 500 and 1500 m (Richardson et al., 1991; Bashmachnikov et al., 2015). Meddies are usually anticyclonic structures, but cyclone meddies are also found in our region of study, presenting vertical structures with high positive anomalies of temperature and salinity (lower than in anticyclonic meddies) and a vertical extension from 500 to 1300 dbar (Richardson et al., 2000; Barbosa Aguiar et al., 2013).

In this work, we analyse more than 10000 Argo profiles combined with 20 years of altimetric data and an eddies' atlas (AVISO+, Sect. 2.3) to characterise the vertical structure of composite mesoscale eddies in the AzC corridor (AzCCo). Furthermore, we explore the concepts of Spice (SPI) and Heave (HEV), relating the observed variations in climatological temperature and salinity fields to eddy trapping, associated with the advection of distinct water masses, and eddy pumping, manifested as the deflection of isopycnal surfaces driven by the internal structure of anticyclonic and cyclonic eddies.

Therefore, the main research questions addressed in this study are as follows: 1) What is the typical vertical structure of eddies in the Azores Current corridor? 2) Which mechanisms - reflected by HEV and SPI anomaly signatures - dominate the generation of internal temperature and salinity anomalies within eddies? 3) How does the presence of mesoscale turbulent structures affect the water column in our study region?

Details of data and analysis methods are described in section 2, and the results obtained are presented in section 3. A brief discussion of the principal aspects of this work is outlined in section 4, and answers to our initial questions are drawn in section 5.

2 Data and methods

2.1 Argo floats

We used 20997 Argo individual profiles (Argo, 2026; https://usgodae.org/cgi-bin/argo_select.pl) inside our study region between 2000 and 2020. These profiles were later pre-processed considering the following criteria: 1) The profiles' data (temperature, salinity, and pressure) were filtered, retaining those with a GOOD quality flag (equal to 1 or 2 according to https://archimer.ifremer.fr/doc/00187/29825/). Adjusted values were used when available; 2) Profiles with their first value below 20 dbar and the last above 1500 dbar were discarded; 3) each profile should have at least 30 vertical measurements, with a depth difference between two consecutive measurements that should be smaller than 25 dbar from the surface to the

100 dbar level, 50 dbar from the 100 to 300 dbar layer, and smaller than 100 dbar below 300 dbar (these intervals were also used in Chaigneau et al., 2011). In the end, 10034 profiles were retained, corresponding to 48 % of the initial number.

The GSW oceanographic toolbox (GSW-OT - www.TEOS-10.org) was used to compute the conservative temperature (CT), absolute salinity (SA), density anomaly (RHO) as well as the mixed layer depth (MLD). All variables were interpolated to 10 dbar levels, and the anomalies of each variable were computed using the World Ocean Atlas 2018 climatology (Boyer et al., 2018 - WOA2018 - https://www.ncei.noaa.gov/archive/accession/NCEI-WOA18) for the Argo period between 2005 and 2017. The climatological data were interpolated in space and time to every Argo profile latitude/longitude and standard depths. In time, the interpolation consisted of finding the climatological profile for the corresponding year-day, using a 12-month spline interpolation. This method was chosen to reduce bias in temperature and salinity mean fields derived from Argo floats' contribution to the climatology computation. This bias could be explained by the extended period of data where Argo floats were not present against the Argo period, leading to interpolations based on low 3D in situ measurement resolutions.

2.2 Vertical isopycnal decomposition

The vertical isopycnal decomposition (hereinafter ISOD) has been applied not only to investigate the warming and/or freshening of specific water masses (e.g., Desbruyères et al., 2022) and ocean heat content variability (Zhang and Yan, 2017), but also to examine the vertical structure of mesoscale eddies and the mechanisms responsible for their internal physical and biogeochemical parameters anomalies (e.g. Frenger et al., 2015; Gaube et al., 2014; Keppler et al., 2024). ISOD separates the contributions of two distinct processes to the generation of CT and SA anomalies: eddy trapping, associated with advection along isopycnal surfaces and quantified by SPI, and eddy pumping, associated with the vertical displacement of isopycnal surfaces and quantified by HEV, which is positive (negative) for downward (upward) isopycnal displacements.

In this work, we use the ISOD to characterise the mesoscale structures and infer which process dominates. Following (Bindoff and Mcdougall (1994) and later Han and Yan (2018), the ISOD equation can be written as:

$$\Delta X|_p \cong X_{SPI} + (-X_{HEV}) + residue \cong \Delta X|_n + (-\Delta p|_n \nabla X) + residual \qquad (1)$$

Where $\Delta X|_p$ represent changes at a pressure level, $\Delta X|_n$ the changes along a given isopycnic surface, $\Delta p|_n$ the difference in pressure for each chosen isopycnal surface reflects the isopycnal vertical displacement ($-\Delta p|_n$- IVD), and ∇X is the climatology vertical gradient. A residual (RES) term is added associated with mixing and/or diffusion, which, for a well-stratified water column, should be near zero.

The ISOD of CT and SA was computed using the same methodology for both the Argo and climatological profiles, following these steps: 1) Neutral isopycnal surfaces (NIS) were computed using the software available at http://www.teos-10.org/preteos10_software/neutral_density.html (Jackett and Mcdougall, 1997) and subsequently interpolated onto a fixed grid. 2) CT, SA, RHO, and pressure were then computed along each NIS. 3) SPI and isopycnal vertical displacement (IVD) were computed as the difference between the Argo and climatological profiles along each NIS. 4) SPI and IVD were interpolated back onto pressure coordinates using the climatological density profiles. 5) HEV was computed as the product of the interpolated IVD and the vertical gradient of the climatological profile. 6) CT and SA anomalies were computed in pressure coordinates. 7) The residual term (RES) was defined as the difference between the total anomaly and the sum of HEV and SPI for each variable. This term can be associated with double diffusion and/or internal mixing in the eddy's boundaries or its interior, or even other processes (like eddy stirring - e.g. McGillicuddy, 2016) that are not explained by the change of the property along the isopycnics (SPI) or due to their deflection (HEV); however, their origin is not the scope of this study and will not be referred to.

In summary, each Argo profile was converted into profiles of CT and SA anomalies, as well as IVD, HEV, and SPI (for both CT and SA). These metrics were then used to construct the eddy composites, which are analysed to assess how mesoscale structures affect the water column in our study region.

2.3 Eddy tracking and Argo co-localisation

The mesoscale eddy trajectory atlas product version 3.2 (hereinafter META2022), produced by SSALTO/DUACS and distributed by AVISO+ (https://www.aviso.altimetry.fr/en/data/products/value-added-products/global-mesoscale-eddy-trajectory-product.html), was used to identify and track eddies in ADT maps using a geometric method, and, in this work, only eddies with more than 10 days of tracking were considered. Absolute dynamic topography (ADT) maps between 2000 and 2020 from the Copernicus Marine Service (CMEMS; https://data.marine.copernicus.eu/) were used. The gridded product is based on merged observations from multiple satellite missions with ¼° spatial resolution and daily temporal resolution. Although the grid spacing is relatively high, the mapped fields are generated through interpolation of along-track measurements, with an effective spatial resolution of ~200 km at mid-latitudes (Ballarotta et al., 2019; Taburet et al., 2019) being structures with ~50 km radius resolved (Chelton et al., 2011, 2019). In our region, the first baroclinic deformation radius is approximately between the values of 30 and 50 km (Chelton et al., 1998), lying near the lower end of the mesoscale spectrum; features at this scale are therefore only partially resolved by the altimetric product, whereas eddies significantly larger are well captured. ADT fields were high-pass filtered using a first-order Bessel filter with a 700 km wavelength cutoff (Mason et al., 2014) to remove large-scale variability and then interpolated in space and time to the locations of the ARGO profiles. These maps were used to superimpose the atlas eddy trajectories. In addition to the detected eddies trajectories, the META2022 contains information of their geometry like the speed contour (contour of maximum circum-average geostrophic speed for the detected eddy) or the effective contour (largest contour of the detected eddy) and kinematic properties such as amplitude (A – positive for both cyclones and anticyclones), radius (R) and swirl velocity (U). Additionally, each eddy turbulent energy was computed ($EKE = \frac{U^2}{2}$). One should note that the algorithm used to track the eddies allows the presence of virtual eddies up to a maximum of 4 days, where no speed contours are computed, and therefore these were not used in the Argo-localisation.

The co-localisation of the Argo floats inside META2022's eddies was conducted, creating a flag for each case where the Argo float emerged inside the speed contour (i.e., the contour of maximum circum-average geostrophic speed for the detected eddy) polygon that defined an anticyclone - ANT, or a cyclone - CYC. Those that were not inside any speed contour were considered outside an eddy - OUT. A total of 2393 Argo (31 %) emerged inside eddies and 7641 outside for the AzC system, while for the AzCCo region, a total of 33 % emerged inside eddies, from which 53 profiles are associated with meddies (see Table 1 for more details). The profiles associated with meddies were filtered accordingly to Richardson et al. (1991) and Bashmachnikov et al. (2015) criteria: the CT and SA anomalies should be above 0.5º C and SA anomalies above 0.2 of salinity for at least 200 dbar between 500 and 1500 dbar. These profiles were later separated from those used in the surface eddies' composites.

Table 1: Number of sampled eddies inside anticyclones (ANT), cyclones (CYC) and outside (OUT) and their number of associated trajectories in the AzC system and in the 3 regions of the AzC corridor.

		ANT	**CYC**	**Number trajectories**		**OUT**
				ANT	CYC	
AzC system	**Total**	**1189**	**1204**	**450**	**439**	**7641**
AzCCo	**R1**	244	268	87	85	1625
	R2	242	209	91	89	1344
	R3	131	116	55	40	649
	Total	**617**	**593**	**233**	**214**	**3618**

2.4 Composite vertical structure

Although different AzC regions along the current main axis have been identified in previous works (Barbosa Aguiar et al., 2011; Silva-Fernandes and Peliz, 2020), here we emphasise the division associated with the main topographic features and extend our analysis to the western flank of the MAR (Figure 1a). Therefore, we will consider three regions: R1 between 20° W and the SWSM chain, R2 from 28° W to the western flank of the ridge following the 2500 m bathymetric, and R3 west of the ridge to 44° W (boxes in Figure 1). To avoid ambiguities when eddies extend across regional boundaries, regional attribution was based on the location of the Argo float sampling the eddy rather than on the eddy centroid position.

After associating the eddies with different regions, a two-dimensional composite (considering the distance of each Argo to the eddy centre) and a vertical median profile (of all Argo profiles inside a region, independently of their position relative to the eddy's centre) of eddy anomalies (CT and SA) and IVD were computed. The latter was used not only to compare the two sign structures to the vertical median of Argo profiles emerging outside eddies along the AzCCo, but also to characterise the vertical structure of meddies as they are found in the eastern part of our domain.

The composites for each region were computed as follows: 1) a normalized distance for each Argo float to the eddy centre was calculated using the ratio (d_A / d_I); the distance of the Argo to the eddy centre (d_A) and the distance of the centre of the eddy centre to the nearest point of the speed contour (d_I) in the azimuth direction of the Argo float; i.e., along the line connecting the eddy centre and the Argo float position (see Figure 2a for more details). Its x (east–west) and y (north–south) components were also computed, and the locations of the Argo profiles sampling the eddies in the regions along the AzCCo are shown in Figure 2b. 2) An optimal interpolation (Barnes, 1973) with 3 iterations is conducted to interpolate each variable onto a regular

0.1x0.1 grid at each depth. 3) Further, to build the composites, we have assumed azimuthal symmetry (i.e., that eddies are circular structures and depend only on depth and distance from the centre). Although this is not verified for all eddies, in terms of statistics, a first decomposition into zonal and meridional mean sections revealed similar vertical structures (not shown).

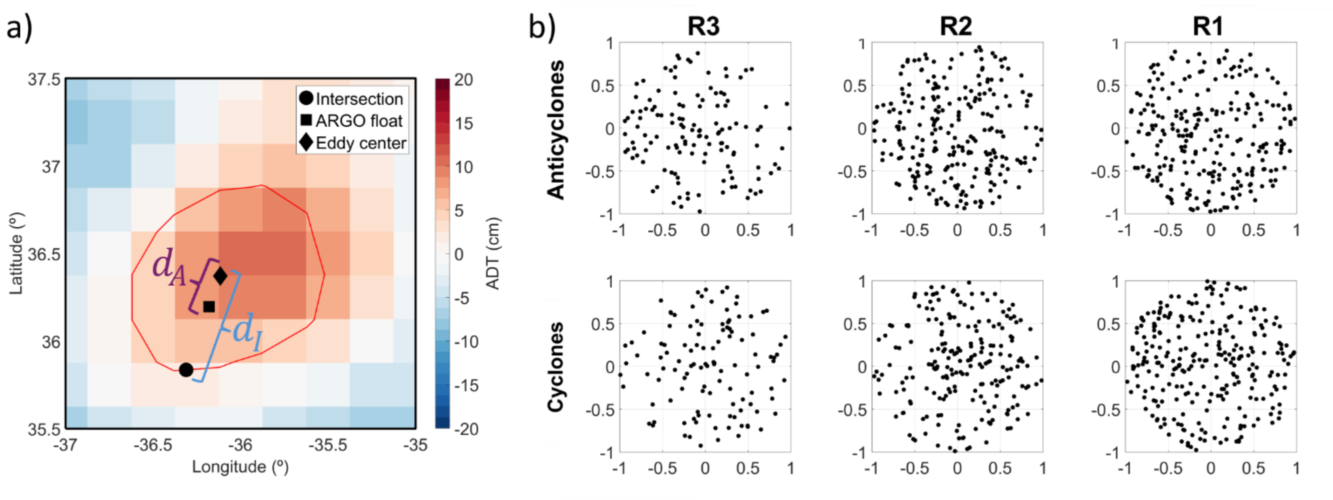

Figure 2: a) Illustration of an anticyclone's characteristics: ADT (colours), eddy centre (black diamond), and the eddy speed contour (red line). The float's position (black square) and the intersection of a line (in the direction of the float azimuth) with the eddy speed contour (black circle) are also shown. The distances d_A and d_I were used to normalise the distance of every float to the eddy centre. b) Normalised distance of the Argo profiles to the eddy centre for all points used to construct the eddy composite for the three AzCCo regions and both sign structures

3 Results

3.1 Argo distribution and eddy field characterisation

The density of Argo profiles in boxes of 1x1 degree for Argo emerging inside anticyclonic eddies – ANT and cyclonic – CYC is presented in Figures 3a and 3c, respectively.

The highest profiles number for both polarities is located east of the SWSM chain, with the maximum for cyclones (24 profiles). Fewer than four profiles are seen below 30° N, especially west of 28° W, with some boxes showing zero Argo floats. Argo floats emerging outside eddies - OUT (Figure 3e) have their maximum also east of 28° W and in the region centred at 31° N, 39° W. Above the AzP and near the SWSM chain, the shallow topography limits the number of Argo in that area. Figures 3b and 3d show the dynamic characteristics (A, L, U, and EKE) of the META2022 sampled by Argo.

Cyclones exhibit larger dispersion of values for all variables, but the median values are similar in both structures: amplitudes of ~5 cm, radius ~80 km, swirl velocities ~20 cm s^{-1} and EKE ~500 cm^2 s^{-2}. ADT and MLD values refer to the Argo location (as in OUT case - Figure 3f), with the cyclones showing larger ADT dispersion (~-60 cm), but with similar median values (~5 cm) and around zero for OUT. MLD medians are ~50 dbar for the three cases, with anticyclones presenting higher values reaching near 500 dbar of depth. Eddies inside the AzCCo have similar median values with lower dispersion. One interesting aspect is the higher median value for the cyclones inside the AzCCo when compared to the full study region.

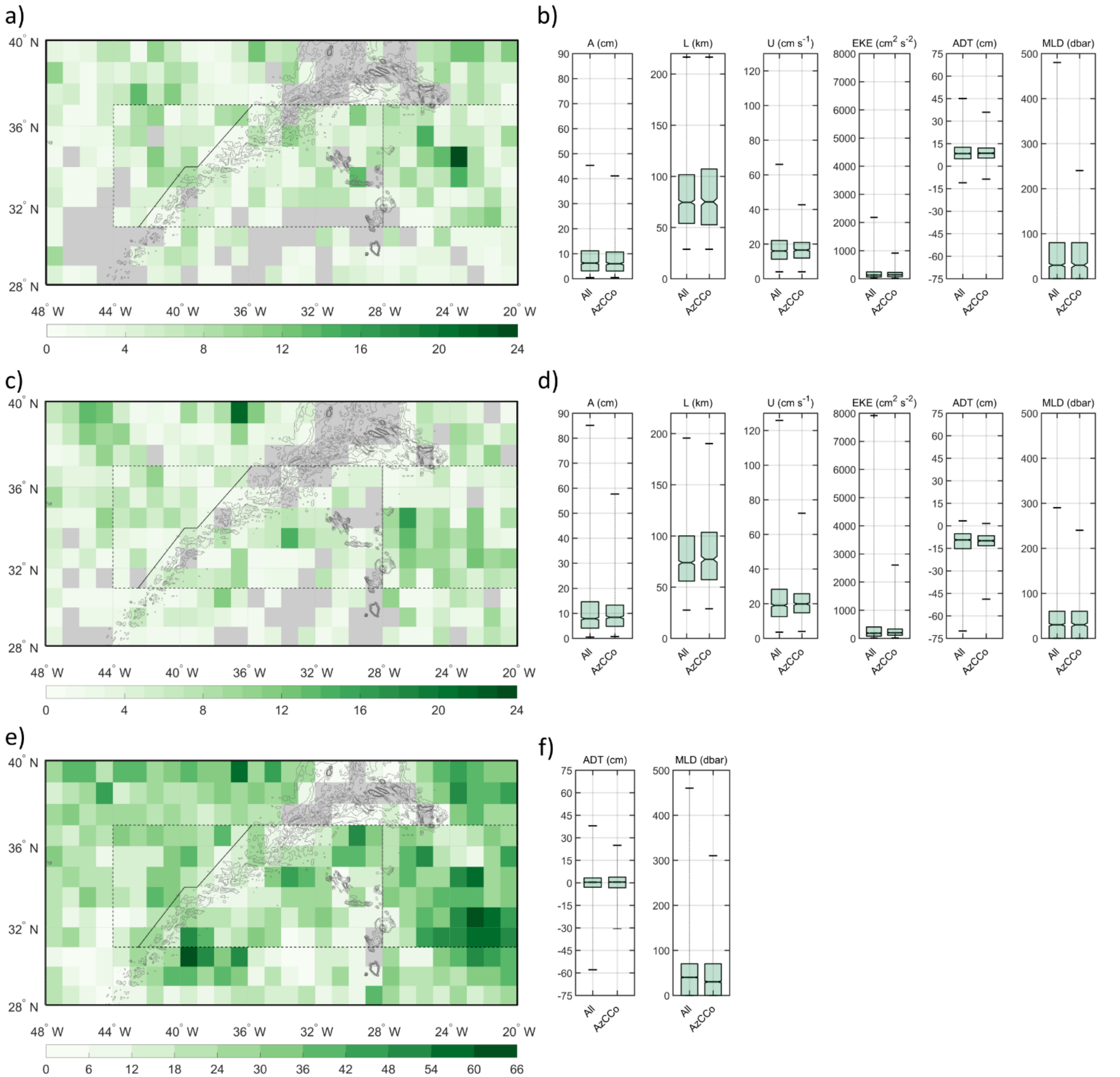

Figure 3: Number of Argo profiles in boxes of 1x1 degree. Emerged inside anticyclones (a), cyclones(b) and outside eddies (e) and their boxplots of kinematic properties for all region and inside the AzCCo: amplitude (A), radius (R), swirl velocity (U), eddy kinetic energy (EKE); absolute dynamic topography (ADT) and mixed layer depth (MLD) for anticyclones (b), cyclones (d) and ADT and MLD for Argo profiles emerged outside eddies (f). All refer to all eddies sampled in our study region and AzCCo to those sampled only inside the AzCCo (R1 to R3).

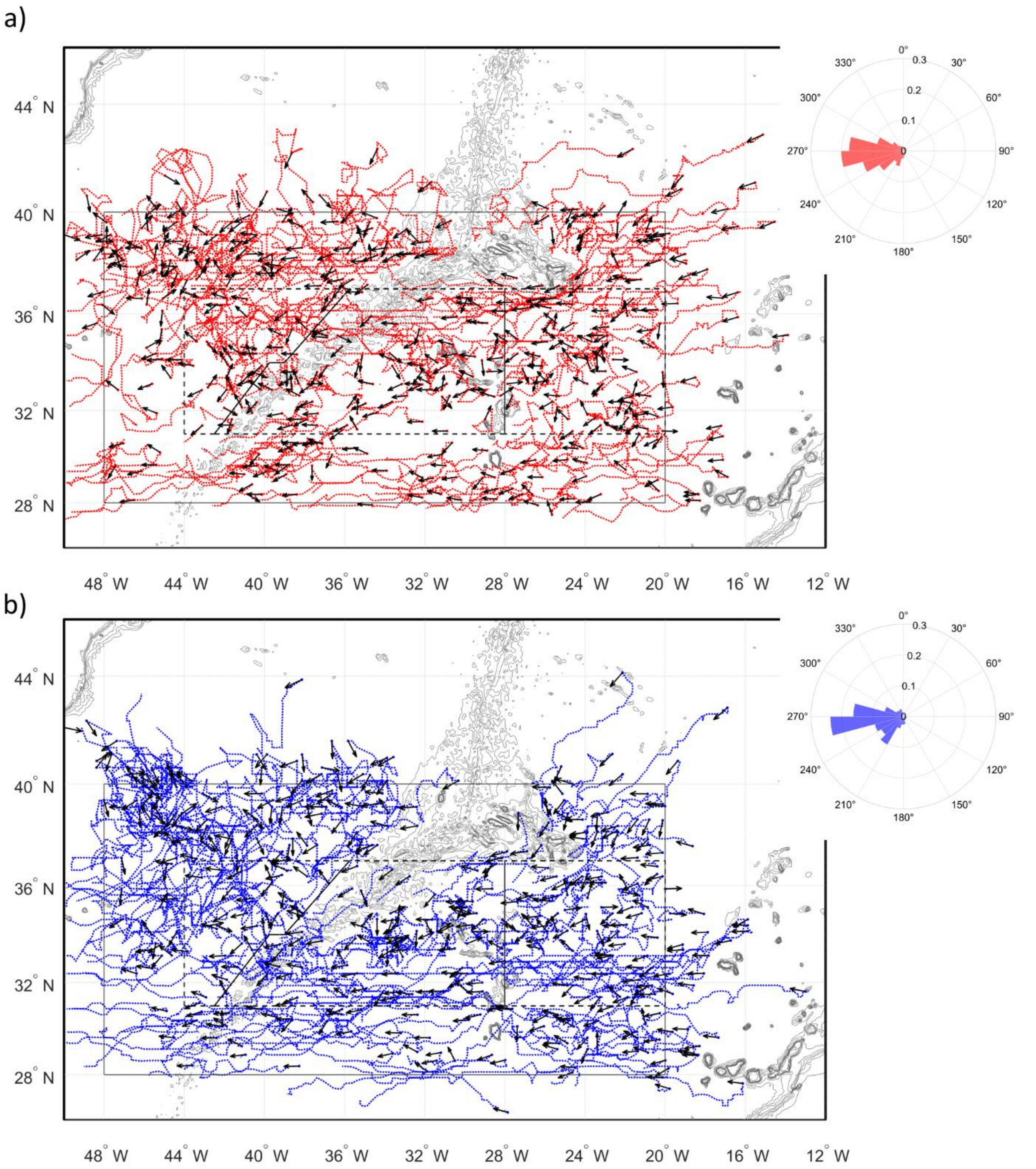

Figure 4: Trajectories (dotted lines) of eddies passing inside the study region (black box) for anticyclones (a) and cyclones (b). Beginnings of detection are represented by points, and the path direction by vectors. The dashed boxes are directly associated with the AzC corridor (AzCCo). The polar graphs represent the relative frequency in each class of the individual trajectory's azimuth, binned in 15-degree classes. The black box represents our study area, and the dashed boxes represent the regions associated with the AzCCo.

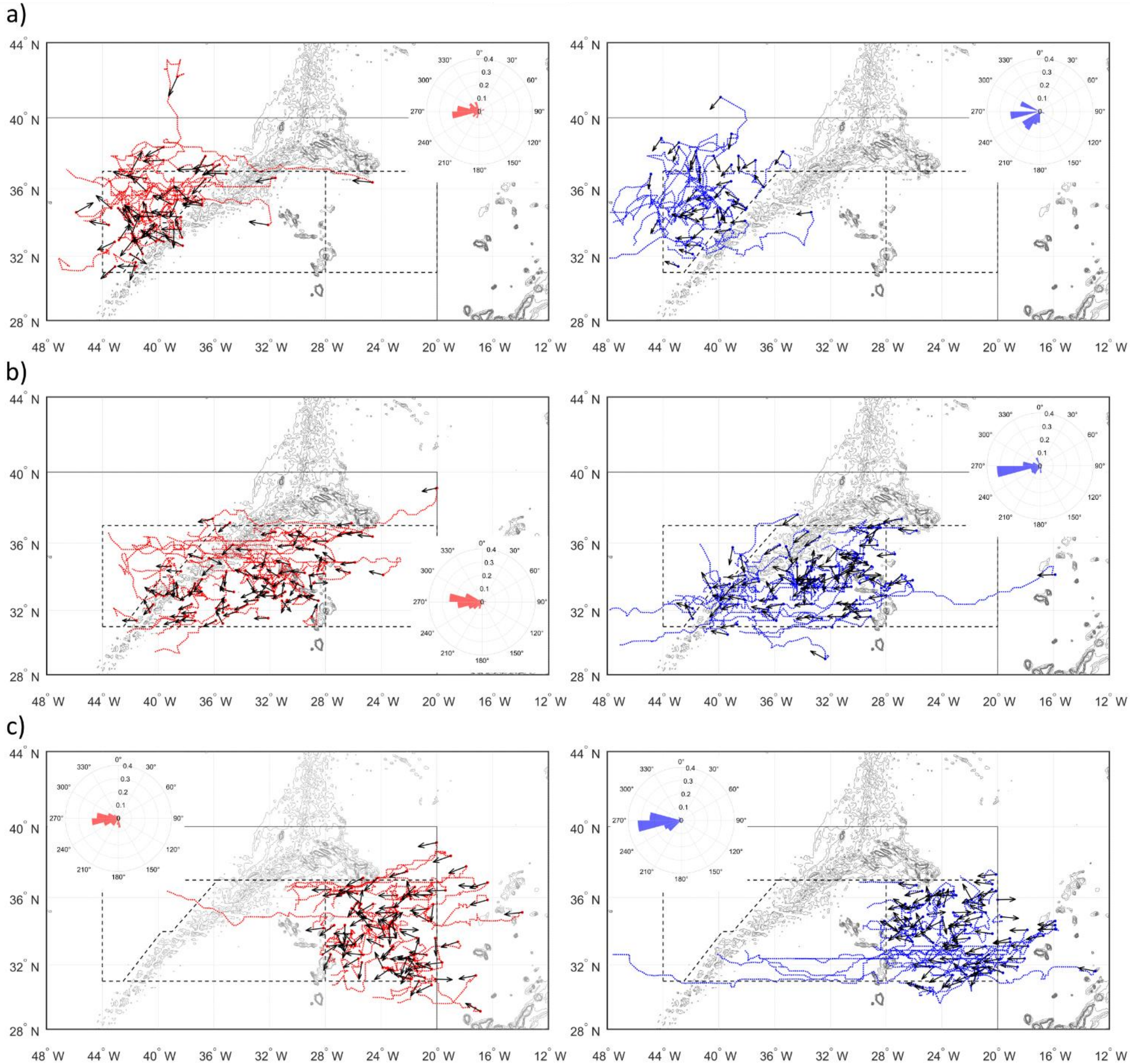

Figure 5: Trajectories (dotted lines) of eddies passing through the AzCCo in region 1 (a), region 2 (b), and region 3 (c) for anticyclones (left) and cyclones (right). Beginnings of detection are represented by points, and the path direction by vectors. The polar graphs represent the relative frequency in each class of the individual trajectory's azimuth, binned in 15-degree classes. The black box represents our study area, and the dashed boxes represent the regions associated with the AzCCo.

Argo sampled eddy trajectories are presented in Figures 4a and 4b, with a total of 450 anticyclonic trajectories and 439 cyclonic trajectories, with 233 and 214in the AzCCo (Figure 5a, b and c), excluding meddy sampled trajectories. Anticyclones have low sampling in two areas: one centred at 31° N - 32° W and west of the MAR at 32° N - 44° W and cyclones, the region above MAR north of 34° N. Both structures present no trajectories above the AzP. Along the AzCCo, the highest trajectories numbers are located north (south) of the current axis (~34º N) for anticyclones (cyclones) in R2, whereas other areas show a more even distribution. Most sampled eddies begin and end (not shown) inside the study area. Their beginning of detection has several different origins (Figures 4a and b), including the region to the northwest associated with the extension of the Gulf Stream or in the east associated with the Madeira (around 32º N) and the Canary Corridors (around 28º N). A group of eddies is tracked from the northeast to the east of the AzP, having the farthest remote origin. Furthermore, the polar graphs in the same figure, show preferential azimuth directions to the southwest (255°-270°) in the case of anticyclones and to the northwest (270°-285°) for cyclones.

Along the AzCCo (Figure 5), 75 % start within their region and 78 % end within it (not shown) (see Table 2 for more information). In R1several cyclones originate origin north or west of Madeira Island, while anticyclones come from the northeast, and both structures present high relative frequencies to the southwest. In R2 most eddies originate locally with only a few eddies tracked from outside the AzCCo. Cyclones have a clear preferential path to the southwest, but several migrate along the ridge. Preferred directions of anticyclones are to the west with some along the ridge. West of the ridge, eddies originate in the north with a southwest path direction for most of the cyclones (see polar graphs) Only three cyclonic eddies originate in R2which indicates that of R3 is influenced by eddies western origins related to the Gulf Stream extensions. The same occur for anticyclones, with more eddies originating in R2 Based solely on path trajectories in R3, it could hypothesise that resulting composites will be biased towards those of the large eddies associated with the Gulf Stream.

Table 2: Number of individual trajectories of anticyclones (ANT) and cyclones (CYC) that pass inside each region: with their start and end of detection inside each region, on the AzCCo and outside the corridor, respectively.

	ANT	**CYC**	**Region**				**AzCCo**				**Outside**			
			Start		**End**		**Start**		**End**		**Start**		**End**	
			ANT	CYC	ANT	CYC	ANT	CYC	ANT	CYC	ANT	CYC	ANT	CYC
R1	87	85	69	66	73	64	2	1	7	13	16	18	7	8
R2	91	89	77	74	71	76	10	9	15	9	4	6	5	4
R3	55	40	29	20	38	27	17	5	7	1	9	15	10	12
Total	**233**	**214**	**175**	**160**	**182**	**167**	**29**	**15**	**29**	**23**	**29**	**39**	**22**	**24**

3.2 Mean zonal and meridional structure

The climatological meridional (Figure 6a) and zonal (Figure 6b) vertical means for the Argo period in the three regions along the AzCCo are shown in Figure 6 left for CT (left) and SA (right).A clear north-south deepening is observed in R1 and R2 linked to the presence of the Azores Front located around 34° N, characterised by colder and fresher waters in the north and warmer and saltier waters to the south. Its signature spans to depths of around 750 dbar in the CT appearing to be shallower in SA. In R3, the same less pronounced pattern is observed. Furthermore, at 1500 dbar, the colder waters (CT < 5° C) intrusion increase the temperature gradient. The same is observed on the meridional mean, with temperature gradients increasing from east to west.

The MW penetration from the east is observed in R1 SA meridional mean, noticeable by the intrusion of waters with higher salinities below 1000 dbar at 20° W. In R2, the same pattern is present at the same depths, linked with the propagation of the MW to the west, also seen in the zonal SA mean. A peculiar aspect of this mean field in R1 is its homogeneity spanning from 750dbar depth to 1000 dbar depth. In R3 at 1500 dbar, the upwelling of fresher waters (SA < 35.3) in association with the lower temperatures highlights the different characteristics between the two basins at depth.

One should note that due to the way regions 2 and 3 boxes were constructed, the meridional mean in R2 (R3) west (east) of 40° W will reflect more the south (north) part of the AzCCo, and in the east (west) the northern (southern) part.

3.3 CT/SA vertical structure

The CT and SA composites along the AzCCo are presented in Figure 7. Meddies´ profiles were separated to better represent surface eddies and their vertical structure is presented in Sect. 3.5. The internal structure asymmetry is observed both in CT and SA composites. The deflection of isotherms and isohalines downward (upward) from the centre of the composite to its boundary in the anticyclonic (cyclonic) case is visible, being more intense for the isohalines.

From east to west, there is an intensification of the CT (Figure 7a) vertical gradient between the east (R1 and R2) and the west (R3) of the ridge, where colder waters (< 5º C) can be observed at the 1500 dbar level, seen in R3 anticyclones and cyclones and in R2 cyclones.

The SA composite (Figure 7b) is highly asymmetrical between the two basins. R1 presents a layer of constant SA (between 35.8 and 35.7) ~750 dbar thick in both sign structures, being deeper in anticyclones. This layer is also observed in R2, presenting less vertical span. R3 shows lower surface SA and intrusion of fresher waters (< 35.2) at the 1500 dbar level. The isohaline deflection is more pronounced in R3 with downwelling (upwelling) of around 75 dbar from the centre to the boundary in anticyclones (cyclones).

3.4 The isopycnal decomposition

The ISOD along the AzCCo both the anticyclonic and cyclonic 2D composites is shown in Figure 8 (HEV, SPI, and RES for both variables, CT and SA, and IVD).

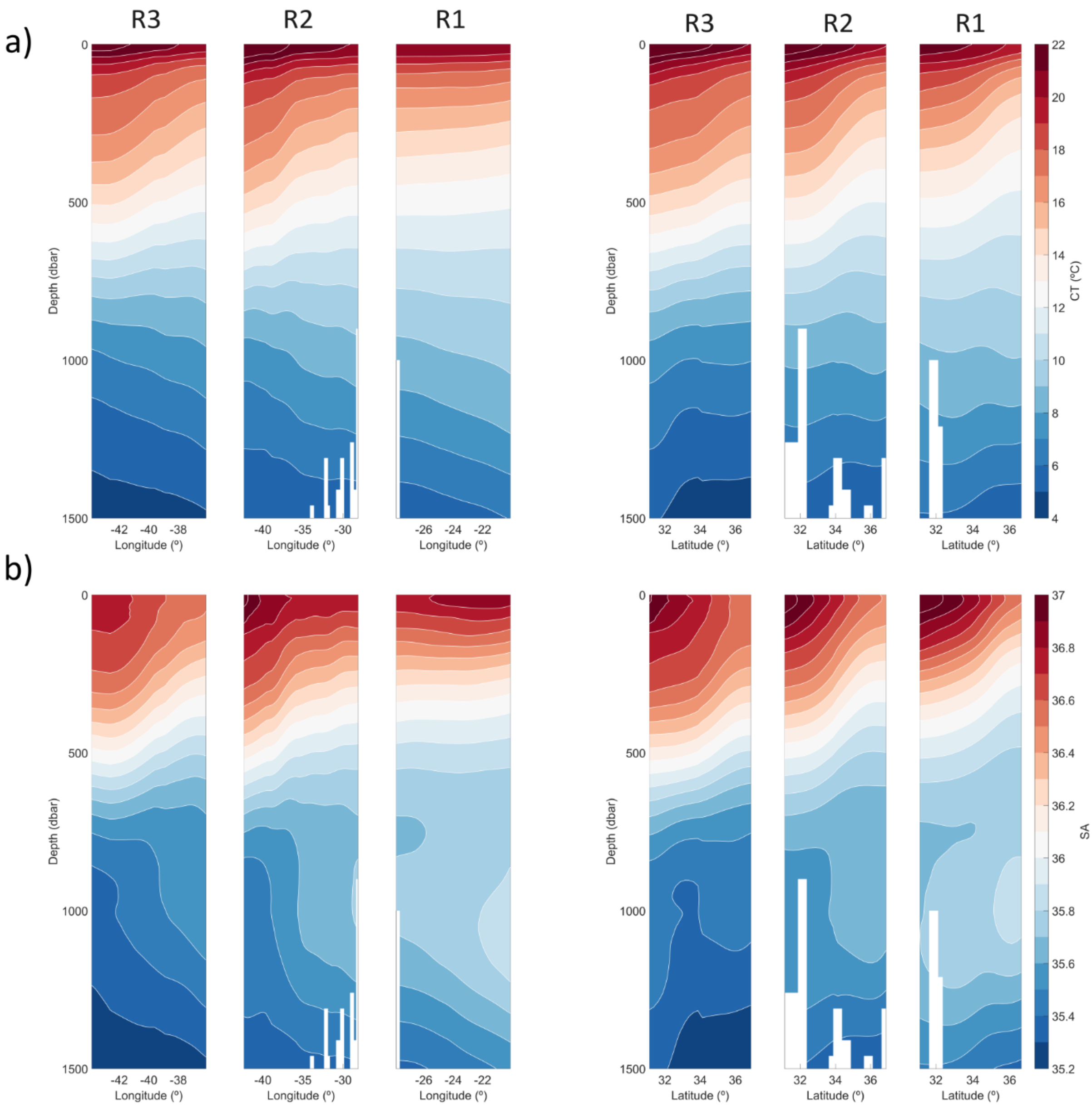

Figure 6: Mean WOA2018 climatology inside the three regions associated with the AzCCo for a) CT and b) SA. On the left are represented the meridional means and, on the right, the zonal. White represents the topography of the region associated with the SWSM chain and the shallower part of MAR.

A significant asymmetry between anticyclones and cyclones is observed in both CT (Figure 8a) and SA (Figure 8b) anomalies vertical structure, magnitude, and sign. While cyclones present a well-defined core, anticyclones present a more vertically elongated structure, especially in R2 throughout the water column.

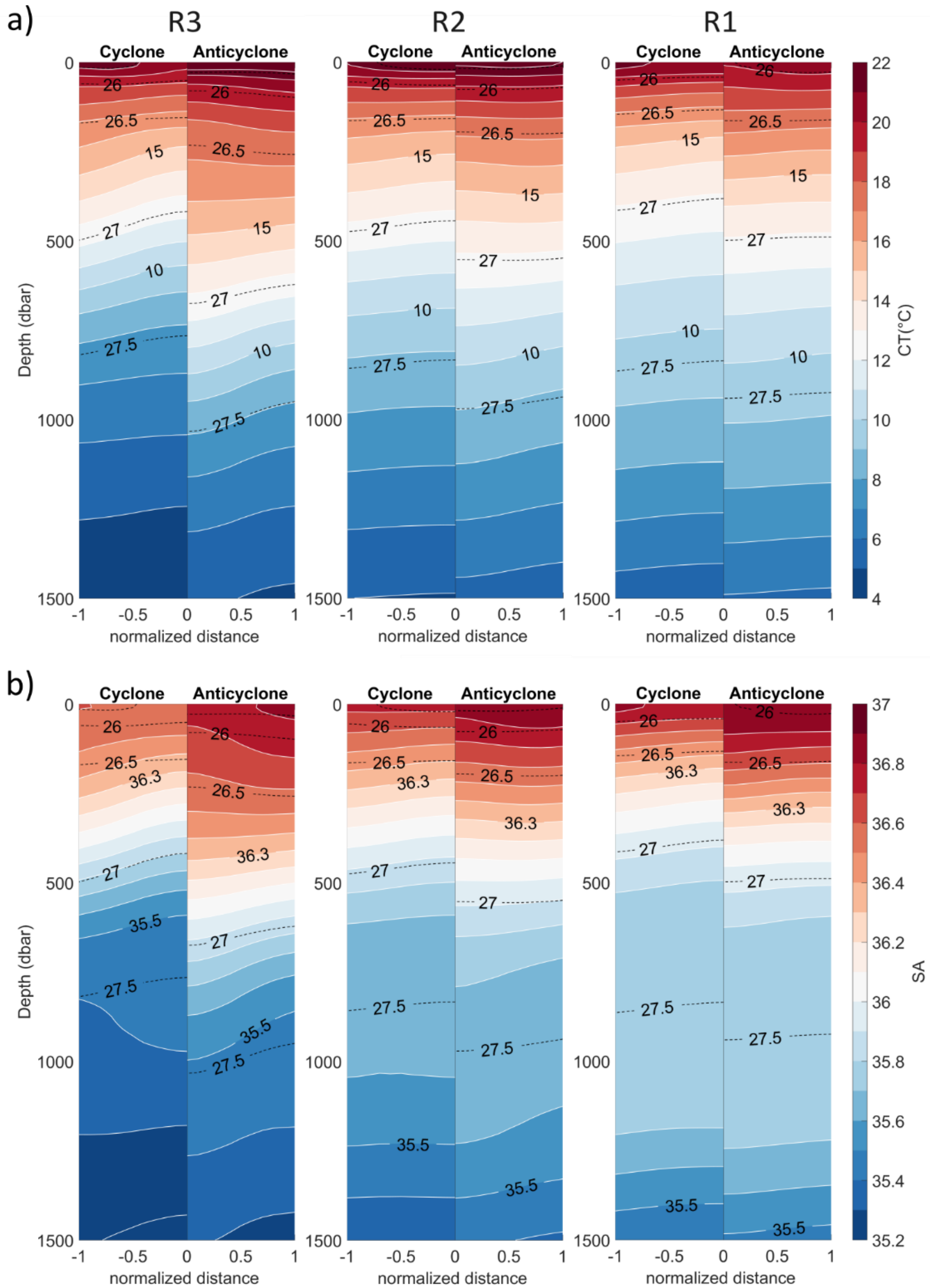

Figure 7: (a) CT radial vertical structure composite for sampled eddies inside R1, R2 and R3 for both anticyclonic and cyclonic structures. Dashed lines represent the density anomaly (kg m⁻³) relative to the surface. (b) The same as (a) but for the SA radial vertical structure composite.

A deepening of eddies' core is observed from east to west (250 to 500 dbar for cyclones and 250 to 750 dbar for anticyclones), being the anticyclones core deeper in R3 (Figures 8a and 8b). Anticyclones have warmer and saltier core (> 0.75° C and 0.1 of salinity), while cyclones show a colder, fresher core (< -2° C and -0.3 of salinity). In R1 for both structures and R2 for cyclones, a minimum of CT anomaly occurs around 1000 dbar. Around the same level and for a deeper vertical extension, the SA anomaly shows a sign inversion associated with the downwelling (upwelling) of the MW in anticyclones (cyclones) due to the deflection (elevation) of the isopycnics. Anticyclone's R2 composite appears as to retain characteristics of both R1 and R3, as it presents an elongated core from surface to the 1000 dbar level, resulting from the sampling in this region being made above the ridge in R2 near the border with R3.

Anticyclones (cyclones) present IVD positive (negative) signs (Figure 8c) reflecting the deflection (elevation) of the isopycnics with a clear asymmetry between structures, being well-defined and stronger in cyclones (below -90 dbar in R1 and R2 and -130 dbar in R3). In R1 and R2 the cyclonic IVD structure is very similar with a slight deepening of the maximum, while in R3, its core presents a more uniform structure from 400 dbar depth to 1500 dbar. The same structure is observed in anticyclones on both sides of the ridge, more pronounced in R2 (> 80 dbar) and R3 (120 dbar). For all regions, the IVD at 1500 dbar is non-zero indicating a deep influence of these eddies on the water column.

HEV (Figures 8d and 8g) dominates SPI (Figures 8e and 8h) in the formation of the CT and SA anomalies. The HEV maxima occur slightly deeper than the anomaly maxima and exhibit the same westward deepening pattern. Furthermore, HEV presents the same sign as CT anomalies, while an inversion appears in SA due to the reversal of the climatological gradient (∇pX - see Equation 1) at around 750 dbar, and therefore the SA IVD spans a smaller vertical extent. Similar to the IVD signal, HEV remains non-zero at depth, supporting the hypothesis that eddies in this region extend deeper than 1500 dbar.

The SPI structure (Figures 8e and 8h) is more complex than that of HEV with cores located shallower in the water column. CT SPI shows that the higher values in the east are confined to the upper 250 dbar presenting a sign inversion at depth with a larger vertical extension. West of MAR, anticyclones present the same sign throughout the water column for anticyclones while the cyclones change signal at 1000 dbar. A similar vertical structure is observed in the SA SPI for both structures.

Although the analysis of the ISOD's residuals (Figures 8f and 8i) is not an objective of this work, they present similar magnitudes as SPI, indicating processes of diffusivity and/or diapycnal mixing or even other processes (like eddy stirring) that are not explained by HEV or SPI. This component is more pronounced in cyclones and west of MAR.

3.5 Median vertical structure

The 10-day mean direction of the sampled eddies along the AzCCo is presented in Figures 9a and 9b, where some preferred directional paths emerge. R1's cyclones have mostly westward directions (255°-285°), while anticyclones present a more dispersed path direction. Contrarily in R2, anticyclones are westward and cyclones have high relative frequencies to the west and southwest. An interesting aspect in R3 is that many eddies present southwest directions in both anticyclones and cyclones (higher in the cyclonic case), indicating northern origin instead of eastern.

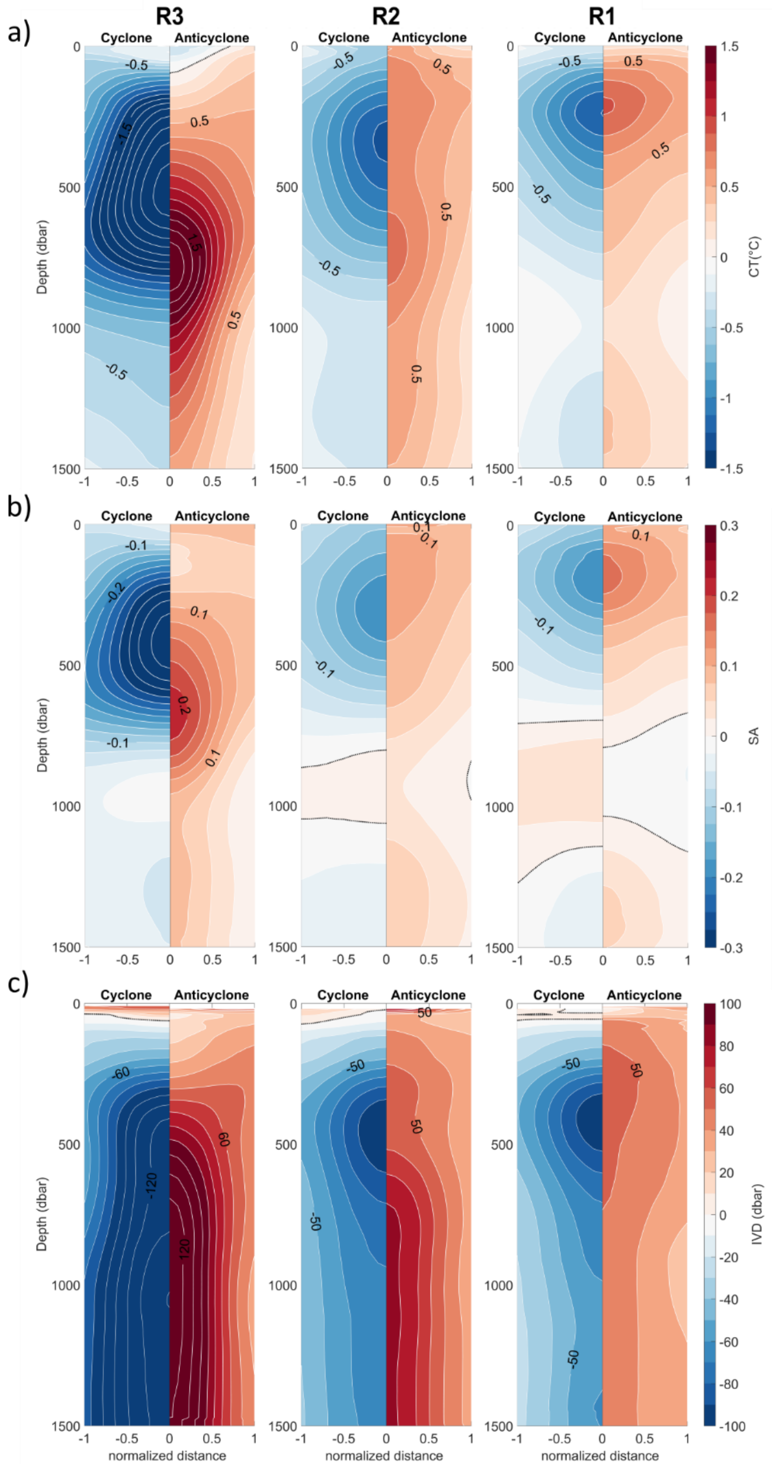

Figure 8: ISOD decomposition: radial vertical structure composite for sampled eddies inside R1, R2 and R3 for both anticyclonic and cyclonic structures. (a) CT anomaly, (b) SA anomaly, (c) Isopycnal Vertical Displacement (IVD). The dotted black line contour represents zero for that variable.

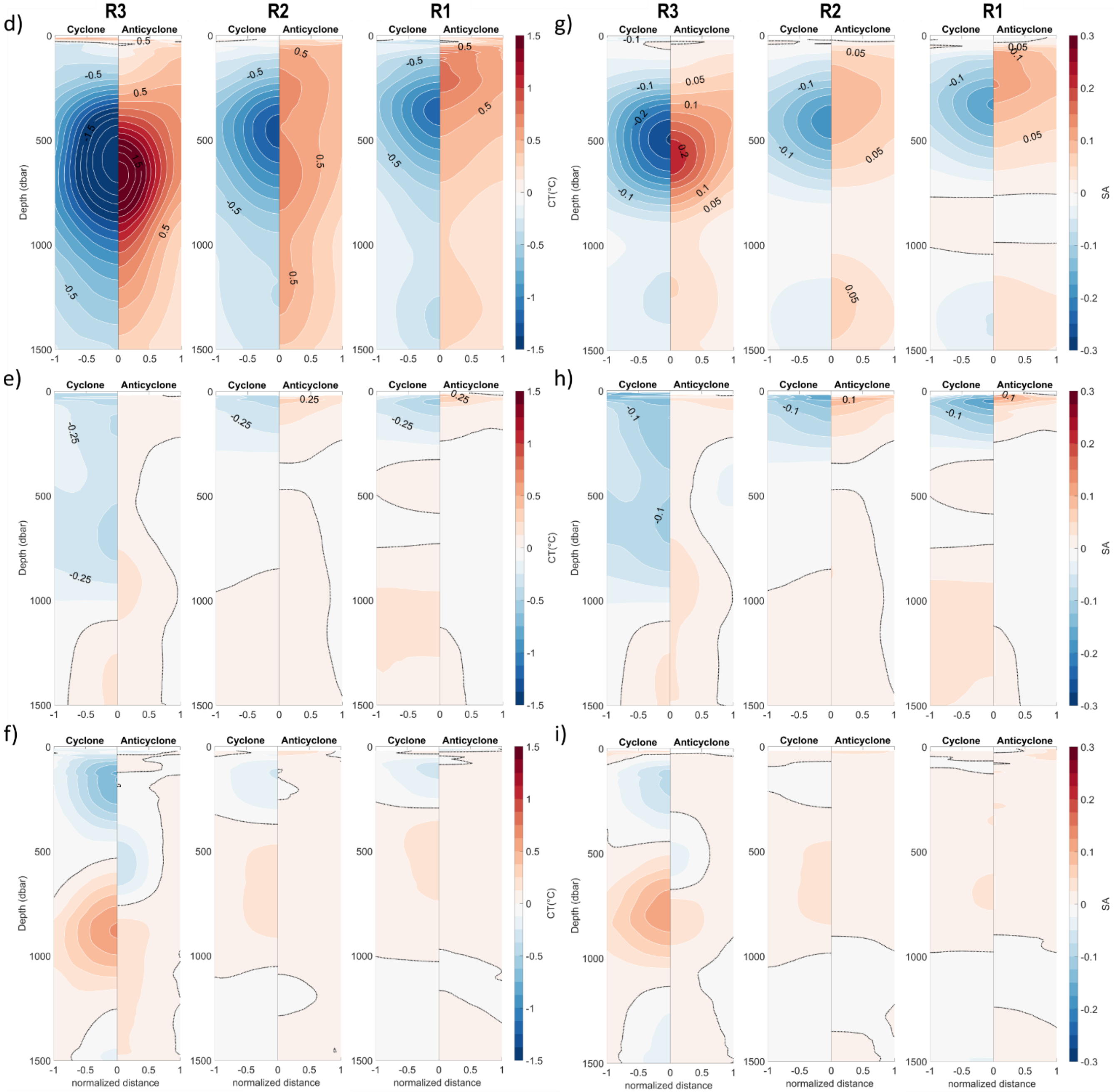

340 **Figure 8 (cont.): ISOD decomposition: radial vertical structure composite for sampled eddies inside R1, R2 and R3 for both**
341 **anticyclonic and cyclonic structures. (d) CT HEV, (e) CT SPI, (f) CT RES, (g) SA HEV, (h) SA SPI, (i) SA RES. The dotted black**
342 **line contour represents zero for that variable.**

343

344

To compare the vertical structure of eddies in the AzCCo with background structure, medians of all profiles inside each region (Figure 9c) were computed and compared to the median of the profiles emerging outside eddies (OUT profiles) for that region. OUT medians for CT and SA anomalies are zero along the AzCCo in the water column, though their percentiles still present significant values (the shaded area of the percentiles is not shown in the figure). This could indicate processes associated with meanders and/or filaments that are not captured by the eddy detection algorithm; virtual eddies (see Sect. 2.4); or even being associated with other processes like Rossby waves.

Asymmetry between anticyclones and cyclones is found along the corridor, being he CT anomaly medians always positive (negative) for anticyclones (cyclones) throughout the water column. Maxima are more defined in the cyclones case, with a deepening in the water column from east to west (from 250 dbar to 600 dbar), and more intense west of the ridge. For anticyclones, their maximum varies from 250 dbar to 750 dbar in the west, increasing also in intensity. In R2, the CT anomaly vertical profile is more uniform than the two other regions.

From east to west, the SA median zero deepens from ~750 dbar in R1 ~1000 dbar in R3 for both structures. Being associated with the MW presence, is visible across the AzCCo and followed by an inversion of the SA anomaly's cyclones sign (from negative to positive) in R1. The same inversion is observed in anticyclones with less intensity resulting from the downwelling of the MW upper boundary by the anticyclone internal deflection of the isopycnics. The same vertical pattern towards zero is exhibited by the CT anomaly in R1, but without the inversion of its median.

The IVD median's vertical structure is almost homogeneous for the anticyclones from the surface to the 1500 dbar, indicating that their internal structure is more uniform, which in R1 and R2 present a maximum above the 500 dbar level. As for CT, the IVD sign is always positive (negative) in anticyclones (cyclones) in all regions, which indicates that the eddies' presence influences the water column to the 1500 dbar. Furthermore, as IVD median are still significant as well as their 90th percentiles (~ 100 dbar in R1 and R2 and ~200 dbar in R3), means that these structures have an influence that can reach depths below that level.

As meddies have a well-known vertical structure which helped us to better understand the SPI and HEV concepts and are therefore analysed in this section. The sampled meddies south of 38º N usually present with some exceptions, western directions (Figure 10a), while those north of that latitude exhibit southwest directions. These meddies are grouped according to their sign at the surface, as the Argo float emerged inside a surface cyclone or anticyclone. A major difference emerges from their vertical structures (Figure 10b): while cyclones are colder and fresher until the 600 dbar depth, anticyclones show a slightly warmer and saltier structure at those depths. Below that level, all present warmer and saltier structures to the 1500 dbar depth, with anticyclones presenting higher anomalies (4° C and 0.8 of salinity against 1° C and 0.25 of salinity) with shallower maximum, while cyclones' median is more constant at depth. The asymmetrical structure of the IVD; anticyclones show clearly high positive values, while cyclones have mainly negative ones, could indicate that we are both in the presence of anticyclonic meddies (positive IVD) and cyclonic meddies (negative IDV). The sampling of meddies by these profiles is corroborated by the CT-SA diagrams (not shown), where higher values of CT and SA are observed, conforming with those associated with meddies. Furthermore, the 10th percentile of the cyclones' IVD presents a sign change at around 1000 dbar, which could indicate that some of these profiles sampled anticyclonic meddies.

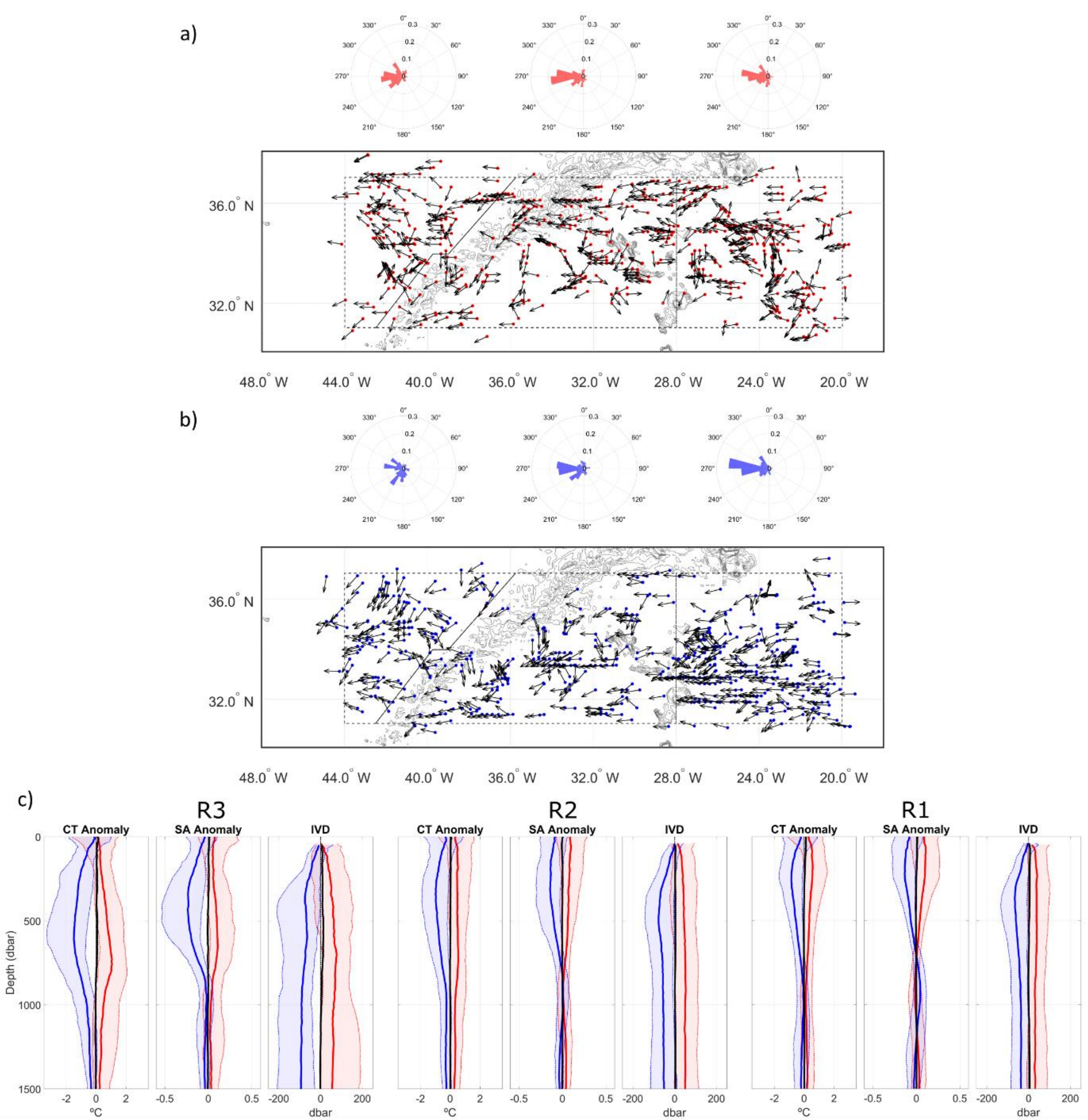

Figure 9: (a) Map of the general direction path (10-day mean) of the sampled eddies along a trajectory inside each region. Location of the sampled eddies represented by points and the path direction by vectors. The polar graphs represent the relative frequency in each class of the individual trajectory's azimuth, binned in 15-degree classes. (b) Median vertical structure of the eddy composite for both sign structures (anticyclone red and cyclone blue) and the median vertical structure of the outside eddies (black) for the three regions associated with the AzCCo: R1 (right), R2 (centre), and R3 (left) for the CT and SA anomalies and the vertical displacement, IVD.

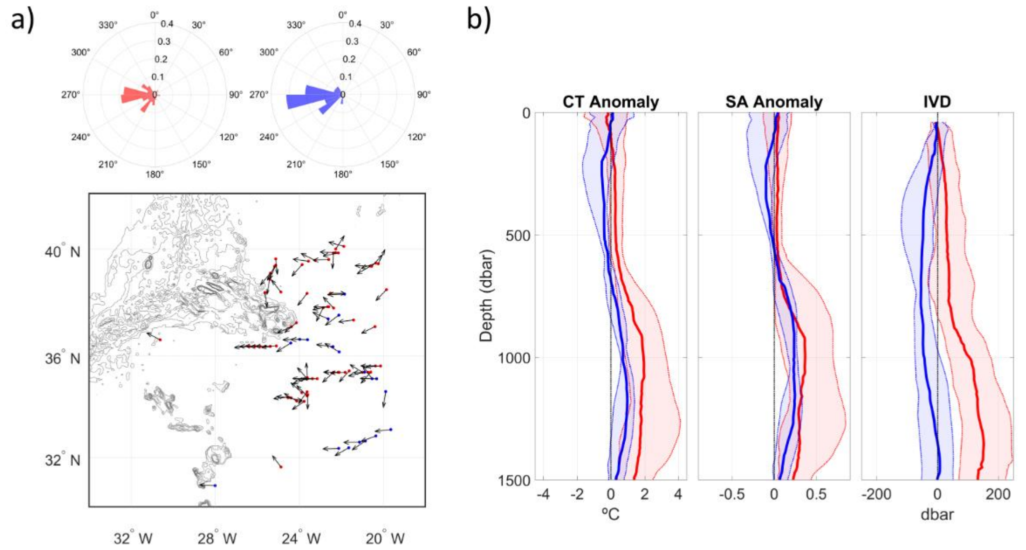

Figure 10: (a) Map of the general trajectories of the sampled meddies (anticyclones red and cyclones blue) for a period of 10 days. The polar graph represents the relative frequency in each class of the individual trajectory's azimuth, binned in 15-degree classes. (b) Median vertical structure of the meddies' profiles for both sign structures (anticyclone red and cyclone blue) for the CT and SA anomalies and the vertical displacement, IVD.

4 Discussion

4.1 West-east eddies' origins

Zonal differences in the eddy's vertical structure along the current main axis are more pronounced between the east and west of MAR, as the ridge acts as a boundary for two areas with very distinct dynamics. From east to west, a deepening of the anomaly's maxima, accompanied by increased intensity (from > 0.5° C and 0.1 of salinity to 1.5º C and 0.2 in salinity) and vertical extension (from 750 dbar to 1250 dbar), is observed both in the 2D radial composites and in the median vertical structure. Anticyclones present warmer, saltier cores, while cyclones have cold, fresh cores with a clear well-defined maximum.

The R1 eddy composite is predominantly local, with some originating in the northeast of the AzP in the anticyclonic case and north of Madeira Island for both structures. In the latter case, these eddies may have two possible origins: either from the evolution of AzC meanders, leading to the formation of eddies that propagate westward, or from the interaction of those with eddies originating in the Canary Upwelling System, which can propagate westward to longitudes as far as 40°W, as previously reported by Pegliasco et al. (2015) and Sangrà et al. (2009). In R3, the sampled trajectories demonstrate directions from the north and east, primarily in the cyclonic case. Furthermore, a migration of eddies to the south on the western flank of the ridge is observed both on the global and the sampled trajectories' azimuths. Ollitrault and Colin de Verdière (2002) reported, based on the trajectories of SOFAR floats launched on each side of the ridge, that eddies are frequently found to travel southward along the western ridge's flank. However, they also found that, after the floats span the western basin between 30° N and 45° N, eddies are also found to travel towards the ridge. Furthermore, Caldeira and Reis (2017), using eddy trajectories tracked on altimetry data (Chelton et al., 2011) and the computation of the zonal and meridional Ekman transport, reported that the Azores Archipelago (in this work represented in the northwest, centre, and southeast of the AzP) is a confluence zone of far-field eddies with different origins. The north-western and central regions are predominantly influenced by the Gulf Stream, filaments, meanders, and eddies, while the south-eastern region is impacted by eddies that are likely to have originated from the meandering AzC pinching. This is consistent with the hypothesis that eddies in R3 are primarily a byproduct of the merging and splitting of mesoscale structures with different origins: those generated in the east and crossing the ridge, and those generated by the evolution of the Gulf Stream branches, migrating to the south along the western flank of the ridge. R2 is a transitional region encompassing the MAR, with eddies originating on both sides of the ridge and above it. The composite vertical structure of eddies in this region exhibits characteristics of both R1 and R3, presenting an elongated core that spans nearly the entire water column. This structure reflects the shallower cores of R1 as well as the deeper cores of R3, influenced by the presence of eddies that may originate from the Gulf Stream system.

4.2 HEV vs SPI

HEV clearly dominates the vertical structure of both CT and SA anomalies on both sides of the MAR throughout the water column, with SPI exhibiting higher values in the first 250 dbar east of MAR and a larger vertical extension on the west. In R1 and R2, HEV presents well-defined maxima for anticyclonic (cyclonic) structures around the 400 dbar (500 dbar) level, showing that the anomalies are mainly generated by the depression (elevation) of the isopycnic surfaces, resulting in the downwelling (upwelling) of warmer (colder) waters and consequent warm (cold) anomalies. West of MAR, the same dominance is observed, reaching higher values and vertical spanning with the same vertical extension observed for the IVD.
Low SPI values in our region can be explained by the fact that most eddies originate and dissipate within the AzCCo. As these eddies travel westward, the CT and SA fields are nearly zonal, so the advected waters retain properties similar to the background, resulting in only minor variations along isopycnal surfaces. In contrast, for meddies (not shown), which advect MW with properties highly contrasting the background, SPI values exceed those of HEV (> 2°C and 0.5 in salinity).
Four mechanisms have been identified as contributing to the transport of physical and biogeochemical properties by eddies: eddy pumping, eddy trapping, eddy-induced Ekman pumping, and eddy stirring. He et al. (2024), using altimetry combined with extensive in situ hydrographic measurements from the World Ocean Database, demonstrated that, at a global scale, temperature anomalies within eddies are primarily impacted by eddy pumping, being consistent with the low values of SPI found in our region. In regions with large horizontal temperature gradients, He et al. (2024) claim the eddy trapping to be relevant, which is the case of the MW by meddies in our region. Frenger et al. (2015) also demonstrates that the sign of the anomaly resulting from eddy trapping is determined by the horizontal temperature gradient in the direction of the eddy movement, which, in our case, is generally to the west. This study also supports our hypothesis that low SPI values are indeed

associated with a meridional gradient of temperature and salinity in the first layer east of the ridge. Contrarily, the high values of meddies' SPI are a result of the sharp zonal gradient of both temperature and salinity.

Several regional studies (e.g., Keppler et al., 2018; He et al., 2023) have shown that eddy-induced anomalies near the surface primarily originate from eddy trapping, whereas eddy pumping is the dominant mechanism at depth. Moreover, Amores et al, (2017), concluded that the mean temperature and salinity anomaly profiles in their northern region (covering part of our study region, south of the current axis and east of the ridge) are dominated by advection in the first 200 m and the vertical displacement of mean isopycnal surfaces below 300 m. The authors also report an eddy signal as deep as 1200 m, which is consistent with HEV values being non convergent to zero at the 1500 dbar and the high values of IVD across all the AzCCo east of the ridge. These findings suggest the potential for these mesoscale structures to exert a deeper influence on the water column. In situ studies previously documented by Pingree et al. (1996) and Mourino et al. (2003) also reported analogous deep signals of eddies have been reported in the range of 100 dbar to 1500 dbar and 200 m to 4000 m depth, respectively.

5 Conclusions

In this study, we analysed the CT and SA profiles of Argo floats emerging within tracked eddies (both anticyclones and cyclones) identified on ADT maps. The main objective was to characterise the vertical structure of mesoscale turbulence along the AzCCo and understand its impact on the water column. Our findings can be summarised as follows.

The vertical structure differences found between the east and the west side of the ridge are associated to the origins of the sampled eddies: while in the in the east, most eddies originate locally, in the west, the majority have origins outside R3 being a combination of eddies travelling from the east and from the northwest, this latter associated to Gulf Stream eddies. This results in more intense anomalies of the westward composites.

When exploring the HEV and SPI signature and intensity, we concluded that: 1) The HEV component is the main contributor to the formation of the CT and SA anomalies, as it exhibits the highest values along the AzCCo. 2) This dominance indicates that most eddy anomalies are generated due to a mechanism of eddy pumping, producing warm and saltier (cold and fresher) anomalies due to the downwelling (upwelling) of the shallower (deeper) isopycnal surfaces in the anticyclonic (cyclonic) eddy interior. 3) SPI shows lower values across the domain, though slightly higher in the upper 250 dbar east of the MAR, reflecting the tendency of eddies tendency to trap different water masses.

Regarding the influence of the mesoscale turbulence in the water column, this work showed that: 1) From east to west, the absolute maximum value of both CT and SA anomalies occurs at increasing depths, from 250 dbar to ~750 dbar. 2) Anticyclones present a more uniform structure while cyclones exhibit a subsurface well-defined maximum. 3) IVD absolute values exceeding 50 dbar from the surface down to 1500 dbar confirm the deep-reaching influence of both anticyclonic and cyclonic eddies. High IVD absolute values (above 150 dbar) across the AzCCo further indicate that these structures could have the potential to enhance vertical advection, not only of heat and salt but also of biogeochemical properties.

Overall, this study confirms that mesoscale eddies along the AzCCo exert a deep influence on the water column, with the differences in their vertical structure linked to eddies' origins and dynamic properties.

Data availability

This study has been conducted using E.U. Copernicus Marine Service Information altimetric data https://doi.org/10.48670/moi-00148. The Argo float data were extracted from https://usgodae.org/cgi-bin/argo_select.pl, and the temperature and salinity 12-month climatology from the World Ocean Atlas 2018 climatology - WOA2018 - https://www.ncei.noaa.gov/archive/accession/NCEI-WOA18.

Code availability

All data analysis was accomplished using MATLAB and Python software. The Python code used to filter the ADT maps is part of the py-eddy-tracker algorithm (Mason et al., 2014), improved in collaboration between IMEDEA (E. Mason) and CLS, freely available under GNU General Public License (https://github.com/AntSimi/py-eddy-tracker/releases/tag/v3.1.0).
The GSW oceanographic toolbox (GSW-OT - www.TEOS-10.org) was used to compute the Conservative Temperature (CT) and Absolute Salinity (SA) as well as the mixed layer depth (MLD), and the package http://www.teos-10.org/preteos10_software/neutral_density.html to compute the neutral isopycnal surfaces.

Author contribution

Conceptualisation: SMSF and AJP. Formal analysis: SMSF. Investigation: SMSF. Methodology: SMSF and AJP. Software: SMSF. Supervision: AJL. Validation: SMSF. Visualisation: SMSF. Writing (original draft preparation): SMSF; Writing (review and editing): SMSF and AJP

Author Disclaimer

The authors declare that they have no conflict of interest.

Acknowledgements

The authors would like to thank the Portuguese Fundação para a Ciência e a Tecnologia for funding this work. A special thanks to Professor Trevor McDougall, Damien Desbruyères, Ricardo Sanchez Leal, and Ying Zhang for all their help on a deeper understanding of the spice and heave concepts and in their computational implementation.

Financial support

Susana M. Silva-Fernandes is supported by the Portuguese Fundação para a Ciência e a Tecnologia (FCT) through the Doctoral Grant PD/BD/142777/2018, within the Earth Systems Doctoral Program of the Faculty of Sciences of the University of Lisbon. This work was funded by the Portuguese Fundação para a Ciência e a Tecnologia (FCT) I.P./MCTES through national funds (PIDDAC) – UIDB/50019/2023 and LA/P/0068/2020 (https://doi.org/10.54499/LA/P/0068/2020), and UID/PRR/50019/2025 (https://doi.org/10.54499/UID/PRR/50019/2025).

References

Alves, M. L. G. R. and De Verdière, A. C.: Instability dynamics of a subtropical jet and applications to the Azores front current system: Eddy-driven mean flow, J. Phys. Oceanogr., 29, 837–864, https://doi.org/10.1175/1520-0485(1999)029<0837:IDOASJ>2.0.CO;2, 1999.

Amores, A., Melnichenko, O., and Maximenko, N.: Coherent mesoscale eddies in the North Atlantic subtropical gyre: 3-D structure and transport with application to the salinity maximum, J. Geophys. Res. Ocean., 122, 23–41, https://doi.org/10.1002/2016JC012256, 2017.

Argo: Argo float data and metadata from Global Data Assembly Centre (Argo GDAC), https://doi.org/https://doi.org/10.17882/42182, 2026.

Ballarotta, M., Ubelmann, C., Pujol, M., Taburet, G., Fournier, F., Legeais, J., Faugère, Y., Delepoulle, A., Chelton, D., Dibarboure, G., and Picot, N.: On the resolutions of ocean altimetry maps, 2018, 1091–1109, 2019.

Barbosa Aguiar, A. C., Peliz, A. J., Cordeiro Pires, A., and Le Cann, B.: Zonal structure of the mean flow and eddies in the Azores Current system, J. Geophys. Res. Ocean., 116, 1–14, https://doi.org/10.1029/2010JC006538, 2011.

Barbosa Aguiar, A. C., Peliz, Á., and Carton, X.: A census of meddies in a long-term high-resolution simulation, Prog. Oceanogr., 116, 80–94, https://doi.org/10.1016/j.pocean.2013.06.016, 2013.

Barnes, S. L.: Mesoscale objective analysis using weighted time-series observations, 657–662, 1973.

Bashmachnikov, I., Neves, F., Calheiros, T., and Carton, X.: Properties and pathways of Mediterranean water eddies in the Atlantic, Prog. Oceanogr., 137, 149–172, https://doi.org/10.1016/j.pocean.2015.06.001, 2015.

Bindoff, N. L. and Mcdougall, T. J.: Diagnosing Climate Change and Ocean Ventilation Using Hydrographic Data, J. Phys. Oceanogr., 24, 1137–1152, https://doi.org/10.1175/1520-0485(1994)024<1137:DCCAOV>2.0.CO;2, 1994.

Boyer, Tim P.; García, Hernán E.; Locarnini, Ricardo A.; Zweng, Melissa M.; Mishonov, Alexey V.; Reagan, James R.; Weathers, Katharine A.; Baranova, Olga K.; Paver, Christopher R.; Seidov, Dan; Smolyar, I. V.: World Ocean Atlas 2018 [2005-2017], 2018.

Caldeira, R. M. A. and Reis, J. C.: The Azores confluence zone, Front. Mar. Sci., 4, 1–14, https://doi.org/10.3389/fmars.2017.00037, 2017.

Chaigneau, A., Le Texier, M., Eldin, G., Grados, C., and Pizarro, O.: Vertical structure of mesoscale eddies in the eastern

South Pacific Ocean: A composite analysis from altimetry and Argo profiling floats, J. Geophys. Res. Ocean., 116, 1–16, https://doi.org/10.1029/2011JC007134, 2011.

Chelton, D. B., DeSzoeke, R. A., Schlax, M. G., El Naggar, K., and Siwertz, N.: Geographical Variability of the First Baroclinic Rossby Radius of Deformation, J. Phys. Oceanogr., 28, 433–460, https://doi.org/10.1175/1520-0485(1998)028<0433:GVOTFB>2.0.CO;2, 1998.

Chelton, D. B., Schlax, M. G., and Samelson, R. M.: Global observations of nonlinear mesoscale eddies, Prog. Oceanogr., 91, 167–216, https://doi.org/10.1016/j.pocean.2011.01.002, 2011.

Chelton, D. B., Schlax, M. G., Samelson, R. M., Farrar, J. T., Molemaker, M. J., Mcwilliams, J. C., and Gula, J.: Prospects for future satellite estimation of small-scale variability of ocean surface velocity and vorticity, Prog. Oceanogr., 173, 256–350, https://doi.org/10.1016/j.pocean.2018.10.012, 2019.

Desbruyères, D. G., Bravo, E. P., Thierry, V., Mercier, H., Lherminier, P., Cabanes, C., Biló, T. C., Fried, N., and Femke De Jong, M.: Warming-to-Cooling Reversal of Overflow-Derived Water Masses in the Irminger Sea During 2002–2021, Geophys. Res. Lett., 49, https://doi.org/10.1029/2022GL098057, 2022.

Dong, C., McWilliams, J. C., Liu, Y., and Chen, D.: Global heat and salt transports by eddy movement, Nat. Commun., 5, 1–6, https://doi.org/10.1038/ncomms4294, 2014.

Frazão, H. C., Prien, R. D., Schulz-bull, D. E., Seidov, D., and Waniek, J. J.: The Forgotten Azores Current : A Long-Term Perspective, 9, 1–14, https://doi.org/10.3389/fmars.2022.842251, 2022.

Frenger, I., Münnich, M., Gruber, N., and Knutti, R.: Southern Ocean eddy phenomenology, J. Geophys. Res. Ocean., 120, 7413–7449, https://doi.org/10.1002/ 2015JC011047, 2015.

Gaube, P., Early, J., Chelton, D., Samelson, R., and Schlax, M.: The Influence of Nonlinear Mesoscale Eddies on Oceanic Chlorophyll, 9569–9569 pp., 2011.

Gaube, P., McGillicuddy, D. J., Chelton, D. B., Behrenfeld, M. J., and Strutton, P. G.: Regional variations in the influence of mesoscale eddies on near-surface chlorophyll, J. Geophys. Res. Ocean., 119, 8195–8220, https://doi.org/10.1002/2014JC010111, 2014.

Gould, W. .: Physical oceanography of the Azores front, Prog. Oceanogr., 14, 167–190, https://doi.org/10.1016/0079-6611(85)90010-2, 1985.

Han, L. and Yan, X. H.: Warming in the Agulhas Region during the Global Surface Warming Acceleration and Slowdown, Sci. Rep., 8, 1–7, https://doi.org/10.1038/s41598-018-31755-1, 2018.

He, Q., Zhan, W., Cai, S., Du, Y., Chen, Z., Tang, S., and Zhan, H.: Enhancing impacts of mesoscale eddies on Southern Ocean temperature variability and extremes, Proc. Natl. Acad. Sci., 120, 2017, https://doi.org/10.1073/pnas.2302292120, 2023.

He, Q., Mo, D., Zhan, W., Cai, S., Tang, S., Zha, G., and Zhan, H.: Thermal Imprints of Mesoscale Eddies in the Global Ocean, J. Phys. Oceanogr., 54, 1991–2009, https://doi.org/10.1175/JPO-D-23-0226.1, 2024.

Jackett, D. R. and Mcdougall, T. J.: A neutral density variable for the world's oceans, J. Phys. Oceanogr., 27, 237–263, https://doi.org/10.1175/1520-0485(1997)027<0237:ANDVFT>2.0.CO;2, 1997.

Juliano, M. F. and Alves, M. L. G. R.: The atlantic subtropical front/current systems of Azores and St. Helena, J. Phys. Oceanogr., 37, 2573–2598, https://doi.org/10.1175/2007JPO3150.1, 2007.

Keppler, L., Cravatte, S., Chaigneau, A., Pegliasco, C., Gourdeau, L., and Singh, A.: Observed Characteristics and Vertical Structure of Mesoscale Eddies in the Southwest Tropical Pacific, J. Geophys. Res. Ocean., 123, 2731–2756, https://doi.org/10.1002/2017JC013712, 2018.

Keppler, L., Eddebbar, Y. A., Gille, S. T., Guisewhite, N., Mazloff, M. R., Tamsitt, V., Verdy, A., and Talley, L. D.: Effects of Mesoscale Eddies on Southern Ocean Biogeochemistry, AGU Adv., 5, https://doi.org/10.1029/2024AV001355, 2024.

Klein, B. and Siedler, G.: On the origin of the Azores Current, J. Geophys. Res. Ocean., 94, 6159–6168, https://doi.org/10.1029/jc094ic05p06159, 1989.

Mahadevan, A.: The Impact of Submesoscale Physics on Primary Productivity of Plankton, Ann. Rev. Mar. Sci., 8, 161–184, https://doi.org/10.1146/annurev-marine-010814-015912, 2016.

Martin, A. P. and Richards, K. J.: Mechanisms for vertical nutrient transport within a North Atlantic mesoscale eddy, Deep. Res. Part II Top. Stud. Oceanogr., 48, 757–773, https://doi.org/10.1016/S0967-0645(00)00096-5, 2001.

Mourino, B., Fernández, E., Etienne, H., Hernández, F., and Giraud, S.: Significance of cyclonic SubTropical Oceanic Rings of Magnitude (STORM) eddies for the carbon budget of the euphotic layer in the subtropical northeast Atlantic, J. Geophys. Res. Ocean., 108, https://doi.org/10.1029/2003jc001884, 2003.

Mouriño, B., Fernández, E., Escánez, J., de Armas, D., Giraud, S., Sinha, B., and Pingree, R.: A Subtropical Oceanic Ring of Magnitude (STORM) in the Eastern North Atlantic: physical, chemical and biological properties, Deep Sea Res. Part II Top. Stud. Oceanogr., 49, 4003–4021, https://doi.org/10.1016/S0967-0645(02)00139-X, 2002.

Ollitrault, M. and Colin de Verdière, A.: SOFAR Floats Reveal Midlatitude Intermediate North Atlantic General Circulation. Part I: A Lagrangian Descriptive View, J. Phys. Oceanogr., 32, 2020–2033, https://doi.org/10.1175/1520-0485(2002)032<2020:SFRMIN>2.0.CO;2, 2002.

Pegliasco, C., Chaigneau, A., and Morrow, R.: Main eddy vertical structures observed in the four major Eastern Boundary Upwelling Systems, J. Geophys. Res. Ocean., 120, 6008–6033, https://doi.org/10.1002/2015JC010950, 2015.

Pingree, R.: Ocean structure and climate (Eastern North Atlantic): In situ measurement and remote sensing (altimeter), J. Mar. Biol. Assoc. United Kingdom, 82, 681–707, https://doi.org/10.1017/S0025315402006082, 2002.

Pingree, R. D. and Sinha, B.: Dynamic topography (ERS-1/2 and seatruth) of Subtropical Ring (STORM 0) in the storm corridor (32-34°N, Eastern Basin, North Atlantic Ocean), J. Mar. Biol. Assoc. United Kingdom, 78, 351–376, https://doi.org/10.1017/S0025315400041503, 1998.

Pingree, R. D., Sinha, B., New, A. L., Waddington, I., Head, R. N., and Nechvolodov, L. V.: Will deep subtropical ring "Storm Physalia" cross the mid Atlantic ridge and reach America?, J. Mar. Biol. Assoc. United Kingdom, 76, 553–567, https://doi.org/10.1017/s0025315400031271, 1996.

Richardson, P. L., McCartney, M. S., and Maillard, C.: A search for meddies in historical data, Dyn. Atmos. Ocean., 15, 241–

265, https://doi.org/10.1016/0377-0265(91)90022-8, 1991.

Richardson, P. L., Bower, A. S., and Zenk, W.: A census of Meddies tracked by floats, Prog. Oceanogr., 45, 209–250, https://doi.org/10.1016/S0079-6611(99)00053-1, 2000.

Sangrà, P., Pascual, A., Rodríguez-Santana, Á., Machín, F., Mason, E., McWilliams, J. C., Pelegrí, J. L., Dong, C., Rubio, A., Arístegui, J., Marrero-Díaz, Á., Hernández-Guerra, A., Martínez-Marrero, A., and Auladell, M.: The Canary Eddy Corridor: A major pathway for long-lived eddies in the subtropical North Atlantic, Deep. Res. Part I Oceanogr. Res. Pap., 56, 2100–2114, https://doi.org/10.1016/j.dsr.2009.08.008, 2009.

Silva-Fernandes, S. M. and Peliz, A. J.: The Turbulent Structure of the Azores Current System: A Statistical Analysis, J. Geophys. Res. Ocean., 125, 1–19, https://doi.org/10.1029/2020JC016327, 2020.

Taburet, G., Sanchez-roman, A., Ballarotta, M., Pujol, M., and Legeais, J.: DUACS DT2018 : 25 years of reprocessed sea level altimetry products, 2014, 1207–1224, 2019.

Treguier, A. M., Deshayes, J., Lique, C., Dussin, R., and Molines, J. M.: Eddy contributions to the meridional transport of salt in the North Atlantic, J. Geophys. Res. Ocean., 117, 1–19, https://doi.org/10.1029/2012JC007927, 2012.

Zhang, W. and Yan, X.-H.: The Subpolar North Atlantic Ocean Heat Content Variability and its Decomposition, Sci. Rep., 7, 13748, https://doi.org/10.1038/s41598-017-14158-6, 2017.